Journal of Visualization, Vol. 10, No. 1 (2007)99-110

3C PIV and PLIF Measurement in Turbulent Mixing

Round Jet Impingement

Reungoat, D. *[1], Rivière, N. *[1,2] and Fauré, J. P.*[2]

*1 TREFLE laboratory 16 Av Pey berland, 33607, Pessac, France. E-mail: reungoat@enscpb.fr
*2 CEA CESTA 12 Av des Sablières 33114 Le Barp, France.

Received 14 July 2006
Revised 3 November 2006

Abstract : The present work focuses on the measurements of instantaneous concentration fields of a passive scalar due to an impinging round jet injection into a liquid filled rectangular tank. Simultaneous measurements of velocity and passive scalar concentration fields have been conducted by using Particle Image Velocimetry (planar 2C and 3C PIV) and Planar Laser Induced Fluorescence (PLIF) techniques. The mixing injection behavior is analyzed for several injection values of depth and flow rate. Results showed the classical developing and self-similar regions of the jet, the mixing layer and the coupled concentration and velocity fields due to impingement. Finally, 3C PIV reveals a 3D flow jet structure which seems to be a swirl that does not disturb 2D analysis.

Keywords : Impinging jet, Turbulent, SPIV, PLIF.

Nomenclature :

d_{inj}	Inlet diameter	mm
h	Impinging distance nozzle (deep)	mm
y_c	Centerline distance (nozzle/measurement point)	mm
Re	Reynolds number	-
V_{mean}	Mean inlet average velocity	m/s
$\overline{V_c}$	Mean centerline velocity	m/s
$\overline{V_c(0)}$	Mean inlet centerline (maximum) velocity	m/s

1. Introduction

Impinging jets are found in different engineering applications like surface cooling, surface coating, liquid atomization and mixing, where the impingement is necessary to obtain a better process efficiency. Because it is one of the basic flow configurations used in many practical and fundamental applications, characteristic behavior of the axisymmetric jet is well known (Law, 2000), for circular and square coaxial nozzles (Bitting, 2001) as well as lobbed nozzle (Hu, 2000), excluding gravity effects (Harran, 1996) or DNS simulations for impinging jets (Hattori, 2004). In literature, review on flow thermal analyses of free jet and impingement jet has been documented by Martin (1977). Turbulent mixing due to jet impingement into a liquid with free surface is frequently encountered in

many industrial and environmental applications. The behavior of a passive scalar in a free surface tank filled with a turbulent jet is thus of great importance.

In turbulence mixing species (ψ) transport is function of both molecular diffusion and transport by the turbulent flow field. To analyze the efficiency of turbulence mixing, simultaneous experimental measurements of velocity fluctuation and concentration fields are needed. In most of previous jet mixing studies, single concentration field measurements were carried out employing Planar Laser Induced Fluorescence (PLIF) and using either local injection or premixed injection methods (Ding, 2003). In general, the PLIF is one of non intrusive experimental techniques that is well adapted to measure concentration fields at low and high Reynolds number during water mixing. For instance, it has been applied to the quantification of chemical reactor in a vortex (Dimotakis, 1993).

To measure simultaneously concentration, velocity and temperature fields with 2 component vectors, several experimental techniques have been first adopted in combustion devices (Fondse, 1983; Brossard, 2004; Bian, 2004; Watanabe, 2005). Some approaches combine Molecular Tagging Velocity (MTV) with LIF for the simultaneous and decoupled planar measurement concerning the fields of the two velocity vector components and concentration in a turbulent mixing layer (Koochesfahani, 2000). With this method, it is possible to measure concentration and velocity fields from the same camera acquisition that ensures time and spatial dependence between these two variables. However, it is not appropriate at high fluid velocity (> 0,5 ms). Other approaches couple L.D.A. to an electrochemical technique (polarographic) in an axisymmetric coflowing jet to obtain axial distribution from one component with time dependent characteristics (Benayad, 2000). In water flow turbulent mixing, major studies in the body of literature involving simultaneous measurement of velocity and scalar quantities have used PLIF for the passive scalar and 2D using Particle Image Velocimetry (PIV) for velocity (Aanen, 1999; Fujisawa, 2004; Hu, 2000).

The involved transport phenomena are complicated as due to the three-dimensional geometry of the present problem and the expected complex turbulent flow field. It should be mentioned that, when the viscosity is low, turbulent advection mixing due to multi-scale vortex motion is dominant. Therefore, measurement analysis of all three velocity components is necessary to clearly understand the dynamic behavior of turbulent flow and the resulting diffusion of the passive scalar. Several combined optical methods are used for 3D turbulence measurements, for example diagnostic Moiré deflectometry combined with tomography for measurement of 3-D turbulent intensity in gas flow (Stricker, 1997). The principles for carrying out a 3D PLIF have been presented by Deusch and Dracos (Deusch, 2000). However, these investigators have not performed any PIV measurements. Moreover, very few 3D PIV measurements have been reported for this application. In the present study, in order to investigate instantaneous diffusion fields of a passive scalar due to round jet injection into a liquid filled square tank, simultaneous measurements of velocity and passive scalar concentration fields have been conducted by PIV (2D and 3D) and PLIF techniques. The mixing injection behavior is analyzed for several injection values of depth and flow rate. It should be mentioned here that few experiments for jet injection mixing are reported in the literature within the present investigation range (5 to 30 diameters along the axis direction).

2. Experimental Apparatus

A test facility was designed to analyze the mixing process due to jet impingement for different impinging distances. A schematic representation of the experimental apparatus is shown in Fig. 1.

A Plexiglas tube (7) of 10 mm inner diameter is used for injection into water filled tank of rectangular cross section (of 590 mm height, 300 mm width and 300 mm depth). The level of water in the tank is maintained constant using a side weir. The jet tube is long enough ($100d_{inj}$) to damp velocity perturbations due to geometrical disturbances and to maintain stable fluid mean velocity profile at the exit of injection nozzle (see Figs. 3 and 7). Measurement instruments include a flow

meter (3) and PIV/LIF system consisting of a Laser device, 2 CCD cameras (12), a Laser sheet (10), optical devices (13) composed of a dichroic mirror that separates LIF and PIV information, and associated software for PIV and LIF treatments (11). Before any experiment, the flow pump is first connected to a closed-loop water circuit (C_1) to ensure homogeneous initial conditions of temperature and concentration in the injected fluid. Then for injection, water flow is pumped to the jet tube using control valve (4).

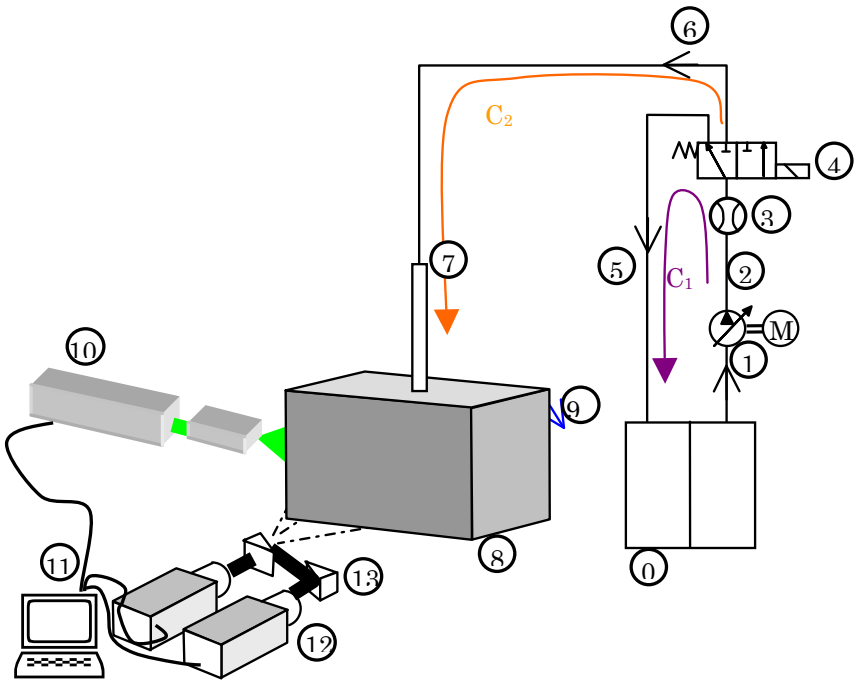

0-reservoir, 1-water pump, 2-pressure line (diameter 10mm eq 0.393in), 3-flow meter, 4-globe or electro valve, 5-closed loop line from by pass with a return line, 6-injection line, 7-transparent round tube (diameter 10mm) ,8-square tank (630x350mm² eq 23.62x13.78 in²), 9-side weir, 10- laser device , 11-PC, 12-CCD cameras 13-optical device.

Fig. 1. Experimental setup.

The jet water is dyed by Rhodamine and seeded with PIV tracers. This dyed and seeded water is then vertically discharged from a round nozzle (the end round tube) placed at the longitudinal cross section centerline of the square test tank (Fig. 1). The nozzle is at a distance from the bottom of the tank large enough to develop all characteristic regions of impingement. The tank fluid was seeded with the same PIV tracers. During injection, the mixing process occurs at the recirculating flow jet interface and the tank fluid.

Measurements are made in the center plane of the jet. Two camera configurations were employed alternatively at the same location with a Nd:YAG pulsed Laser as the excitation source. All images are treated for the specific wavelengths.

At first, to capture simultaneous PIV 2D and PLIF images, the two CCD cameras are used for the same measurement area in the tank to ensure simultaneous concentration and 2D velocity field measurements. The Laser sheet illuminates both PIV tracers and fluorescent dye in the measurement field. A CCD's optical device (11) divides the scattered and emitted luminosity from the experimental scene to the synchronized cameras, each one, catches respectively the fluorescent light emission and the particle diffusion at different wavelengths.

Afterwards both cameras are also used to make 3C PIV measurements for the same experimental conditions with the classical stereoscopic arrangement (Raffel, 1998).

The flow conditions are summarized in Table 1. Unfortunately the dissipation rate from Kolmogorov scale in the case of a free jet cannot have a constant value due to the expansion flow shape as in tubes. That is why we have done the calculations for this coefficient based on L. K. Su (1998) comments and results from Friehe et al. (1971) in the self-similar region of a round jet. In our case the Kolmogorov length scale λ_k follows the linear curve which ranges from 35 to 70 μm in the self-similar region.

The spatial resolution of the measurement is controlled by the digital characteristic of the

camera and the arrangement of optics. This pixel resolution is in the range of the Kolmogorov eddies and sufficient to investigate the passive scalar transport which is attributed to the large scale eddies. This resolution must be associated with the classical software PIV treatment subpixel displacements which are estimated from Gaussian peak with a common accuracy of 0.05-0.1 pixel (Raffel, 1998).
To study the effect of the turbulent diffusion, differential and thermal diffusions must be eliminated. Differential diffusion could be generated from differential solid particle concentration and molecular dye. The water jet is seeded at the same concentration than the water tank to ensure a low particle relative density to avoid developing inertial separation between injected water and stagnant one (Saylor, 1993). For 30 μm diameter particles of Rilsan the inertial response time τ_p equals $9{,}55.10^{-7}$s. This condition is proportional to the one needed for the accuracy of the measurement in PIV in turbulent flow. In order to respect this turbulent diffusion, the fluorescent dye concentration is very small, as it was first observed in the same configuration by Saylor (1998). No inertial effects, as well as negligible molecular effect, can be assumed at a concentration less than 0.001 % for low Reynolds (see Schmitt number table 1).

Thermal diffusion could result from natural convection, and could be eliminated if the injected fluid temperature is the same as the stagnant one during experiment.

Table 1. Experimental conditions.

Case	Jet mean velocity V_{mean} (m/s)	Volume Q (l/min)	Deep h (mm)	Schmidt number Sc	Prandtl number	Reynolds number Re
1	1	4.7	160			10,000
2	1.8	8.1	130/150/230	3841	6.74	17,900
3	2.35	11.1	150/230	3841	6.74	24,526

Like other authors experimented before, since the particles are approximately of the same size than the latter scale, they cannot accurately track the motion of these smaller scales. The integral time scale can be estimated from the ratio of the jet radius, d_{inj}, and the tube mean centerline axial velocity V_{mean}. For the field measurements, the total acquisition time is 120s giving 50-120 independent samples. The total number needed for convergence is about 600 samples. Therefore all analyses are done with several experiments in the same conditions.

Fluorescence experiments need a calibration curve built from different homogeneous concentrations in the tank. This calibration curve also includes the static optical defects and background. Indeed, errors committed by a constant non-homogeneous spatial distribution of light can be corrected with a linear calibration function. Therefore the calibration function allows taking into account the defects of spatial distribution from a non-uniform lighting and static optic aberrations between laser sheet and CCD sensor.The linear range of the mean intensity value is observed and the maximum dye concentration is found to ensure that measurements are done in the linear part of the curve. Under these conditions, the fluorescence signal can be related to the local concentration as shown by Eq.(1).

$$I(i,j) = \psi(i,j)C(i,j) \quad (1)$$

$\Psi(i,j)$ = scalar concentration at pixel location (i,j), and $C(i,j)$ = conversion coefficient for the pixel (i,j)

Experiments were done with Rhodamine 6G and one with Rhodamine B under a maximum concentration of 40 μg/l. The background intensity emission distribution was established by taking several images of the measurement area with "pure" water and PIV particle. It must be noticed that the fluctuation of the recorded intensity has not been included as Guillard did (Guillard et al., 1998). But, calibration was performed for 15 image of a homogenous concentration which establishes the very low fluctuation of standard deviation (< 8) in the range of 500 – 700 grey levels. In these conditions, we consider that the laser light energy fluctuations do not generate any defect on the mean concentration value.

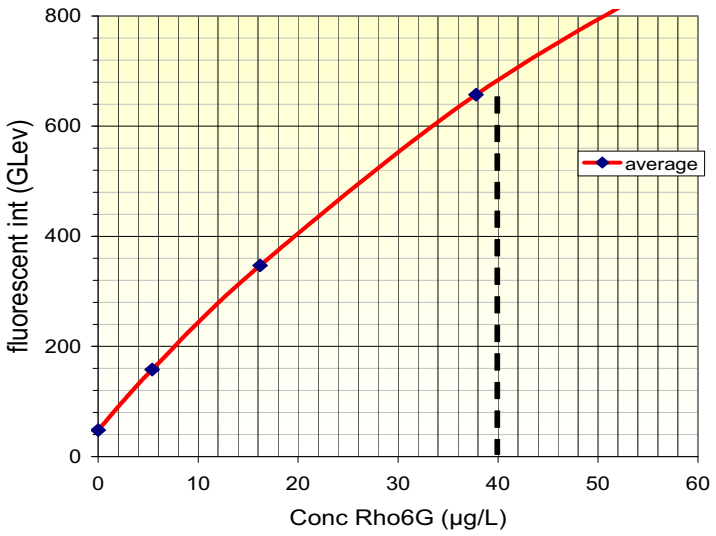

Fig. 2. LIF calibration.

3. Results

Velocity fields from 2C PIV are used to analyze flow structure and turbulence dissipation. Concentration fields from PLIF measurements are compared to velocity in the whole structure like 3C PIV measurements. These results are discussed in the following section. First a general picture of the flow structure (Fig. 4) is presented to identify different flow regions. Then, detailed results and analysis are developed for each characteristic region.

3.1 General Flow Structure

In a first step to verify there is no significant disturbance from the injection line, the injection front was observed. As it was previously noticed (Batchelor, 2001), the injection front develops a vortex ring. At a starting injection jet pulse, with a velocity injection value of 0.45 m/s, the classical ring due to interactions between "pure" water and dyed water is observed (see Fig. 3). Because this ring keeps its symmetrical structure along a distance of $5d_{inj,}$ the injection is considered symmetrical. These results combined with the profile velocity (Fig. 6) verify that no significant disturbances are generated in the injection line. To observe injection at higher pump flow rates, the valve is changed to a smoother, but manual one, that makes only established injection analyses possible.

The small aspect ratio combined with a high Reynolds number of the tube flow ($10{,}000 < Re < 30{,}000$) induce inevitably a confined and 3D injection. A sample velocity and the simultaneous concentration field of Rhodamine is shown in Fig. 3(b). The flow field along the wall that can be subdivided into four zones including a stagnation zone and three wall-jet zones: I II III see Fig. 4 (Chen, 2005).

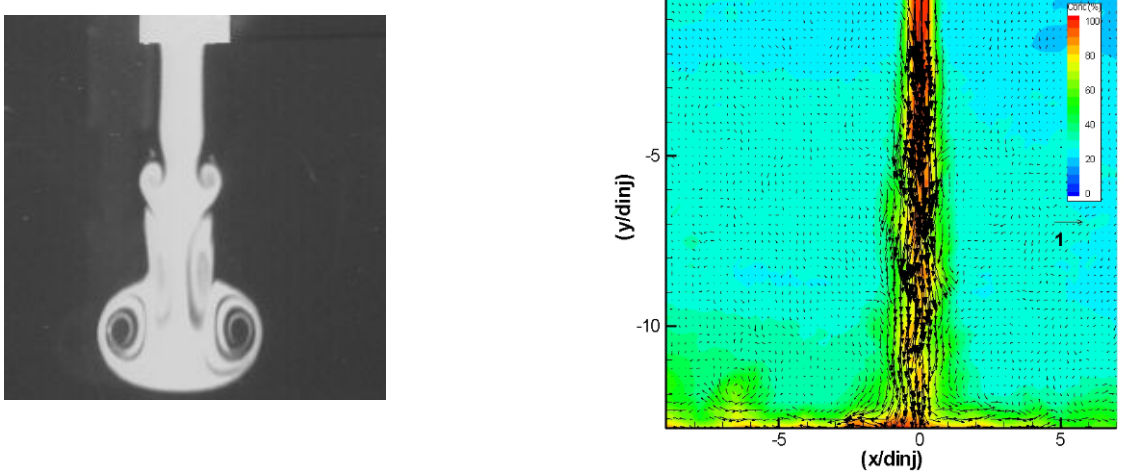

(a) Starting injection (V_{mean} = 0.4 m/s). (b) 2D velocity field PLIF (V_{mean} = 2.3 m/s)

Fig. 3. Flow conditions.

This jet mapping is in agreement with both previous observations from literature for free jet studies and impinging jet. From impinging axisymmetric jet analysis, the flow structures can be

divided into three characteristics regions: the free jet region, the impingement flow region, and the region of radial outside flow (wall jet region). The free jet region can be subdivided into three zones: the potential core zone, the developing zone, and the self similar zone (also called developed zone or zone of established flow ZEF).

Figure 4 shows the ZEF and developing zone located in the deflecting region. It must be first noticed that the self similar zone for a free jet is defined in the range of y_c/d_{inj} = 30 to 120 that couldn't be completely developed in our conditions, and secondly that the potential core length depends on the magnitude of the injection velocity.

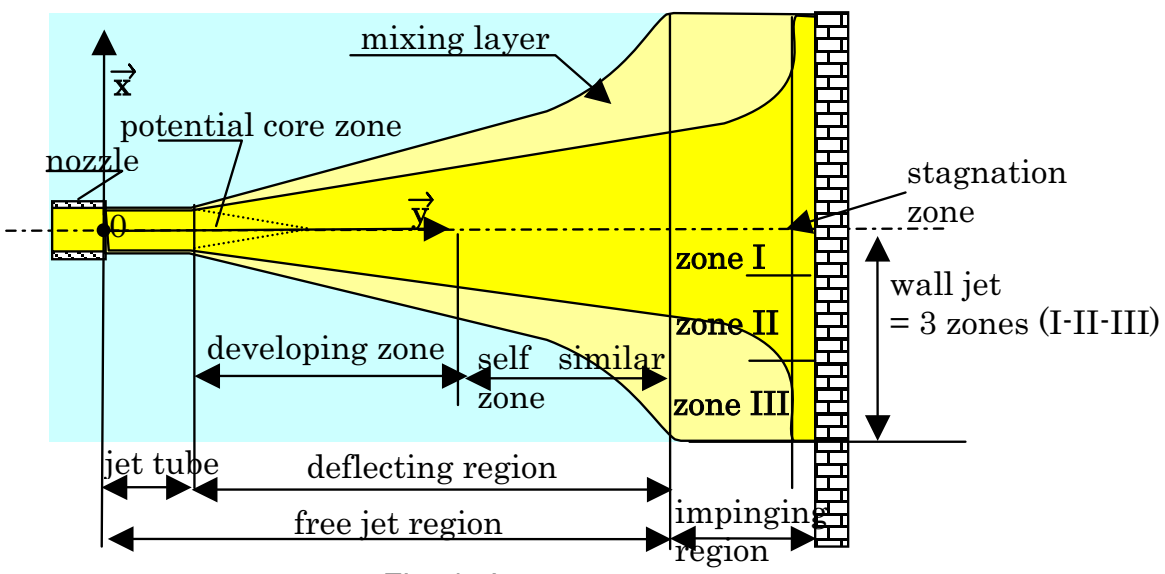

Fig. 4. Jet map.

3.2 Potential Core

Law and Wang (Law, 2000) have performed combined measurements with Digital Particle Image Velocimetry (DPIV) and planar laser induced fluorescence (PLIF) to analyze the mean time and turbulent mass transport in the mixing process of a round jet injection in a stagnant fluid. In their studies, they compare the obtained velocity and scalar results to accurate measurements from the studies of Hussein et al. and Panchapakesan and Lumley who performed similar experiments in an air jet with several measurement techniques (Hot-Wire Anemometer, Laser Doppler Anemometer). In Fig. 5, these previous results and our measurements are compared. The behavior of the mean axial velocity and concentration along the jet centerline as a function of the distance from the nozzle is shown in Figs. 5 and 11 for the range of 2 to 50 diameters.

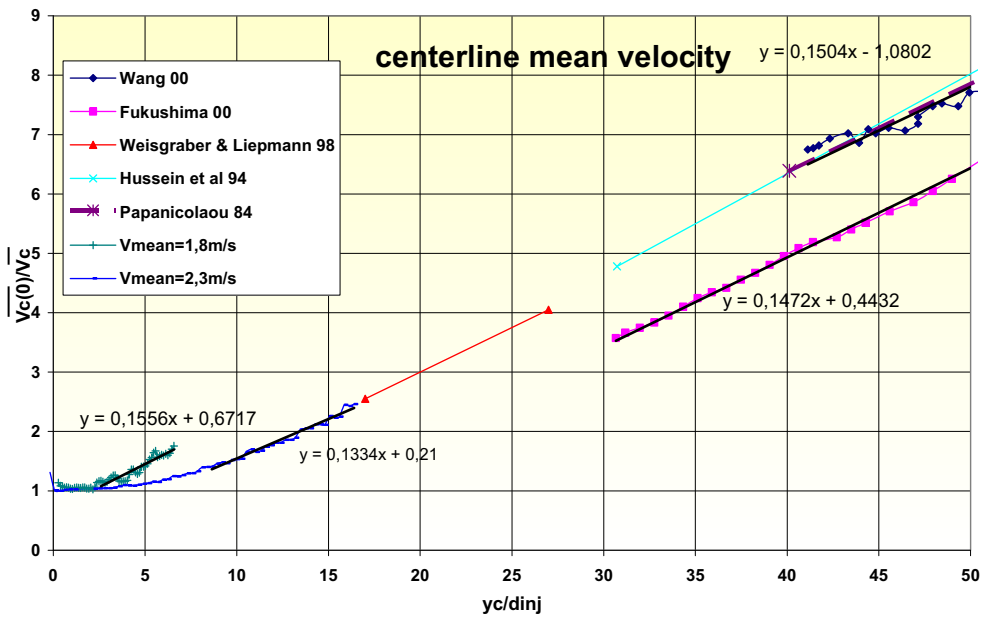

Fig. 5. Centerline jet mean velocity.

The earlier description of the jet structure is reproduced. First, we observe that tube velocity profile is kept in the same order in the potential core region as it was previously found in earlier works (Fig. 6 -curve 5&4). The dimensional characteristics of the region is found again near 6-7 diameters from nozzle exit for axisymmetric jet and 4-8 slot widths for slot jets. However, inside this region, it has been observed a different shape in the flow structure between the injected fluid and the fluid in the tank: within a short distance from the nozzle, the jet is conserved smoothly cylindrical.

3.3 Developing and Self Similar Zone

After the developing zone, the velocity profile is fully developed and jet attains a self-similar behavior better fitted by a Gaussian velocity distribution (Reichardt, 1942).

As it can be shown in Fig. 5, in this region the velocity decay proportional to y^{-1} is in accordance with the previously observed law (Weisgraber and Liepmann, 1998; Fukushima, 2000) (Eq.(2)). We observe in this region a break in the velocity decay that switches to follow a non-proportional to y^{-1} function with a high level of oscillation (end of curve not drawn).

$$\frac{\overline{V_c(0)}}{\overline{v}_c} = \frac{1}{k_{jw}} \times \frac{y_c}{D_0} \qquad (2)$$

$\overline{v}_c$ = mean centerline velocity y_c = centerline distance (from nozzle to measurement point)

In the proportional region the velocity decay coefficient (k_{jw}) depends on the velocity injection (see Table 2) but it is contained in the range of 6.6 to 7,7 from observed results of Law and Weisgraber (1998) respectively 6.48 and 6.2 (see Table 3).

Table 2. Decay coefficients from jet injection.

k_{jw}	k_{jwg}	Re	Injection depth
7.1	121	17,900	150 mm (5.9 in)
6.6 **[6.6]**	110 **[89]**	17,900 **[12,700]**	130 mm (5.1 in) [law]
6.8	121	24,526	130 mm (5.1 in)
7.7		24,526	230 mm (9.44 in)

This ZEF can be observed too with the cross-sectional variations of the mean axial velocity profile along the centerline. In Fig. 6, measurements at different locations are plotted, where we can observe that at a distance of $6d_{inj}$ the self similar profile of the velocity can be found and fitted with the curves from the Eq.(3) (Law, 2000). The coefficient k_{jwg} agrees well with previous results of experimental works from Law and other authors (see Tables 2 and 3).

$$\frac{\overline{v}}{\overline{v}_c} = \exp\left[-k_{jwg}\left(\frac{r}{y_c}\right)^2\right] \qquad (3)$$

$\overline{v}$ = mean velocity value at r; r= radial distance

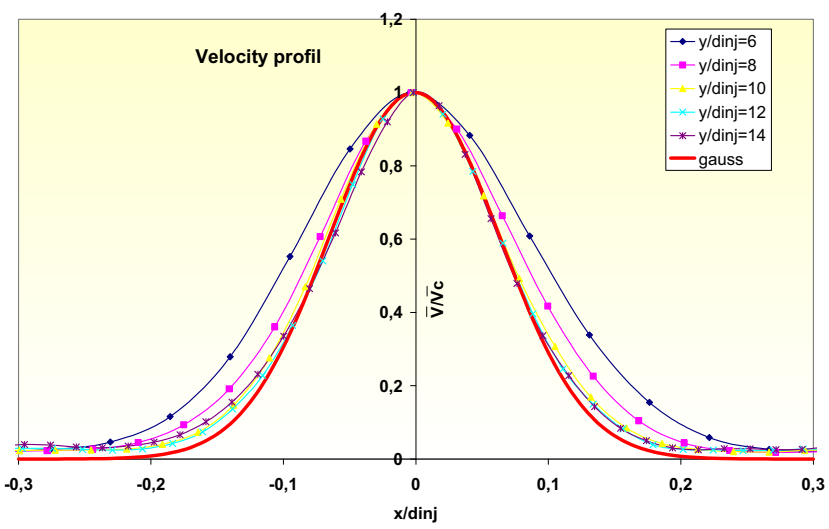

Fig. 6. Centerline mean velocity self similar profile (h = 150mm V_{mean}= 1.8 m/s).

3.4 Impinging Region

In the impinging region, as it can be seen from simultaneous velocity and concentration fields (Fig. 7), the jet flow is re-directed from an axial into a radial direction. So the impinging region is composed of the classical stagnation zone. The radial velocity diffusion expends axisymetricaly from the stagnation zone to entire volume of the tank with a constant low angle.

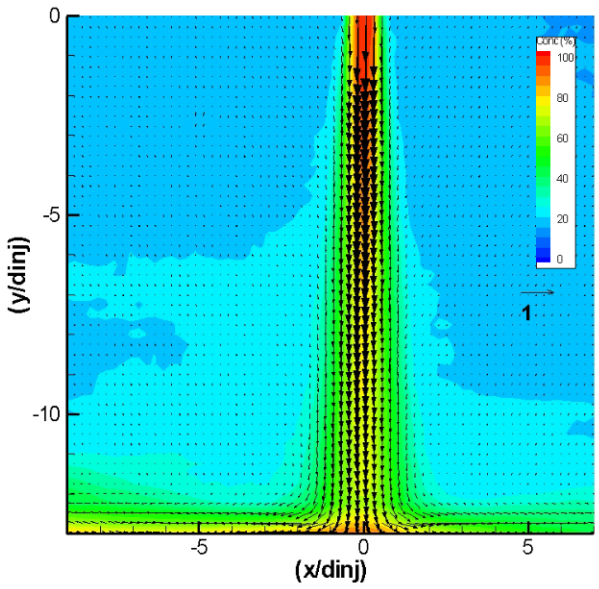

Fig. 7. simultaneous concentration & velocity field in the Wall region (case2 h = 130 mm).

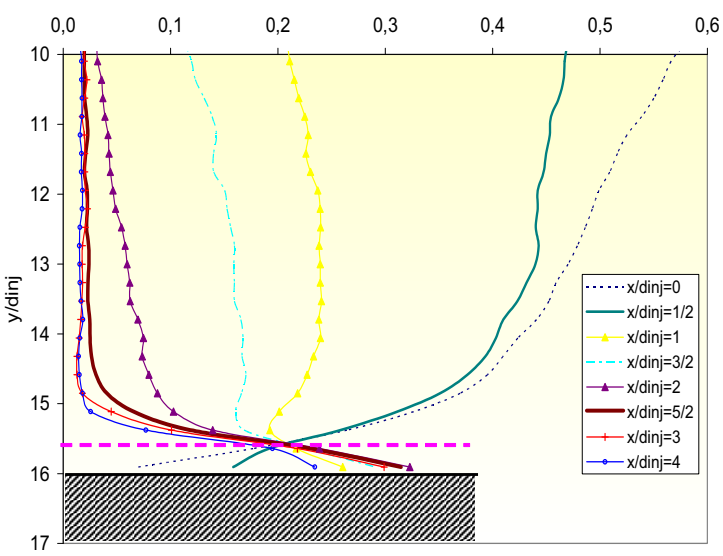

Fig. 8. Velocity Profile in the Wall region (case1 h = 160 mm).

Figure 8 shows the mean velocity profiles along the wall axis at various distances from the jet axis (x/d_{inj} = 0, 0.5, 1, 1.5, 2, 2.5, 3, 4). It can thus be observed that at a distance of y/d_{inj} = 0.5 the mean axial flow is redirected towards the wall direction corresponding to the boundary layer.

Like Nishino results (Nishino, 1996) the normalised axial component profile follows the Gaussian distribution, even in the immediate vicinity of the wall (y/d_{inj} = 15.91 corresponds to 0.09 the normalized distance from wall). Closer to the wall, the axial velocity decreases down to zero at the stagnation point. The axial mean velocity, the radial velocity and turbulent intensity are all presented in Fig. 10. Like in previous works (Nishino, 1996), we found a sharp peak of the turbulent intensity (V_{xrms} = u') around x/d_{inj} = 0.5 far from the wall. Near the wall, it can be also observed too that at a distance of x/d_{inj} = 1 the radial component of the jet flow becomes important enough to be the major part of the velocity magnitude.

The stagnation region is an interesting area for heat dissipation. In this region, the concentration is caught. The concentration profile is reverse to the mean velocity magnitude profile (see Fig. 9). The addition of the concentration distribution with the velocity profiles reveals a stagnation area around the stagnation point. It can be established at x/d_{inj} = +/-1 in the radial direction (Figs. 9-10) and $y = 0.5d_{inj}$ (Fig. 8) in the centreline direction matching the above observation from the boundary layer (Fig. 9). This area is also observed in the measured concentration field (Fig. 13).

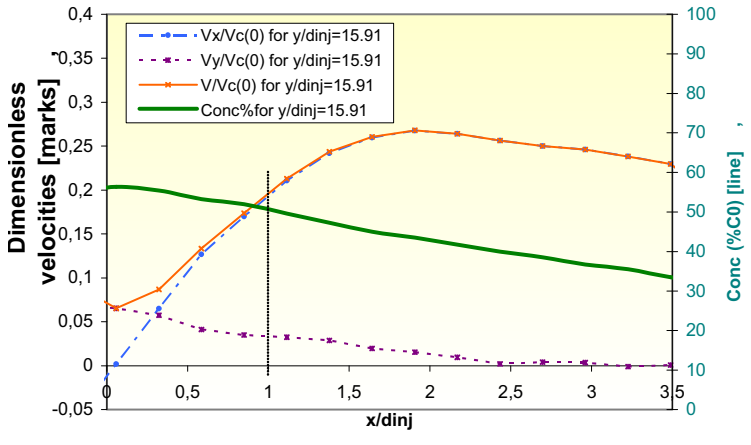

Fig. 9. Impinging region (case1 h = 160 mm).

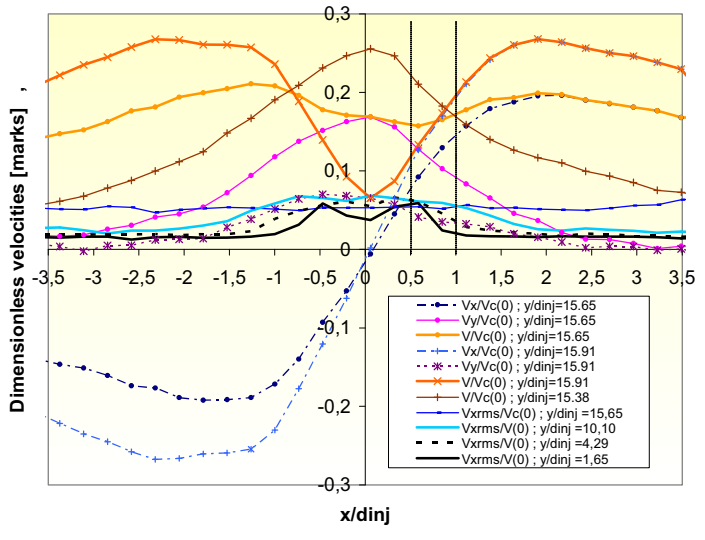

Fig. 10. Velocity in Impinging region (case1 h = 160 mm).

3.5 Mixing Structure

In another way, the concentration distribution structure in the impinging jet cross section is compared with the results from Guillard's works (Guillard, 1998). In this jet three loci from three average measured concentrations were considered 90 %, 25 %, 10 %). The 90 % locus determined the border line of the jet core (see Fig. 11). The mixing layer thickness is defined between the 25 % locus and the 10 % locus. This layer is naturally very different between the two experiments due to the distance from the wall. It is interesting to notice that the 10% loci from each experiment are quite similar even if the distance from the wall is very different. The curvature of the edge of the jet is reproduced with the same proportion in the two experiments but the start of the deflection zone is located at a different distance: $1.2d_{inj}$ (Guillard, 1998) versus $3d_{inj}$ for our experiment.

Table 3. Experimental conditions in different jet studies.

Author	Method	Fluid	V_{mean} (m/s)	d_{inj} (mm)	Tank cross section	Deep xd_{inj}	Dist.nozzle/ wall	Re	k_{jw}	K_{jwg}
Law	PIV/LIF	Water	2.52	4.5	$222d_{inj}$ x$666d_{inj}$	200	$889d_{inj}$	12,700	6.69	89
Fukushima	PIV/LIF	Water	2	1	$110d_{inj}$ x$110d_{inj}$	300	$300d_{inj}$	2,000	6.8	85
Guillard	LIF	Water		33	$9.6d_{inj}$ x$9.2d_{inj}$	9.8	$5d_{inj}$	11,000		
Weisgraber	PIV	Water		25.4	$47.2d_{inj}$ x$47.2d_{inj}$	94.5	$30d_{inj}$	16,000-5,500	6.7-6.3	100-80

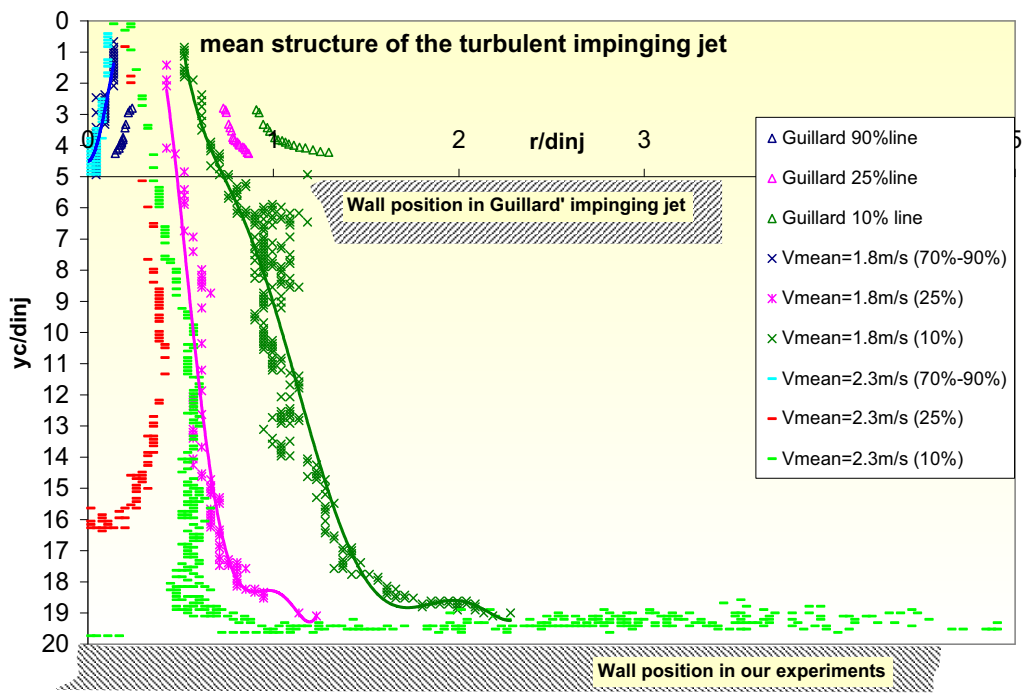

Fig. 11. Mean concentration structure of the turbulent impinging jet.

Flow injection from axisymetrical jet generates vertical structures in the impinging region. The following Figs. (Fig. 3(b)) show the vortical structure which rolls along the wall from instantaneous 2D velocity field in the case of $h = 13d_{inj}$. Although the boundary layer is found to be $0.5d_{inj}$ wide, the classical eddy rolling along the wall can be $2d_{inj}$ large.

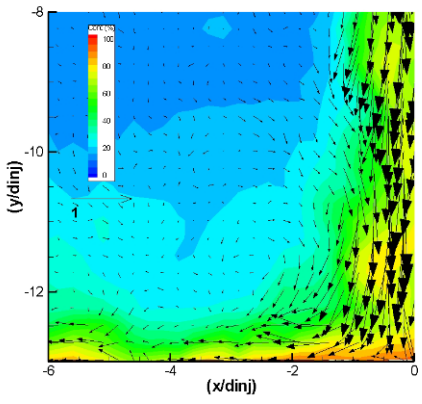

Fig. 12. Zoom from Fig. 3(b).

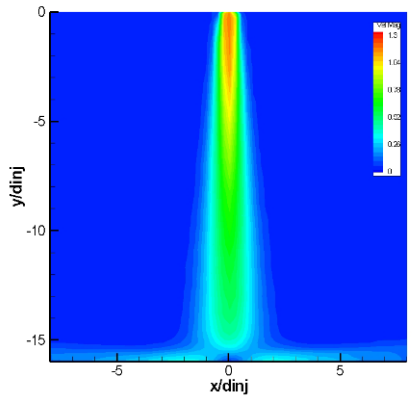

Fig. 13. Mean concentration.

3.6 Stereoscopic Velocity Field

In comparison to the jet structure from the velocity and concentration fields, the three velocity fields components obtained with the stereoscopic device are analyzed. The results reveal a symmetrical distribution from the location plane of the perpendicular velocity component. This distribution is associated with the Kelvin-Helmholtz eddies instability of the mixing layer. Comparison between 2C velocity fields from the standard PIV measurements and the stereoscopic PIV measurements (SPIV) are in good agreement with standard axisymetrical velocity distribution (Fig. 15(a)). As it can be also observed in the three components field (Fig. 15(b)), velocity structure is organized in local "dipole" of the third component at surrounding expansion jet seems to define a swirl structure of eddies (Figs. 14(a) and (b)).

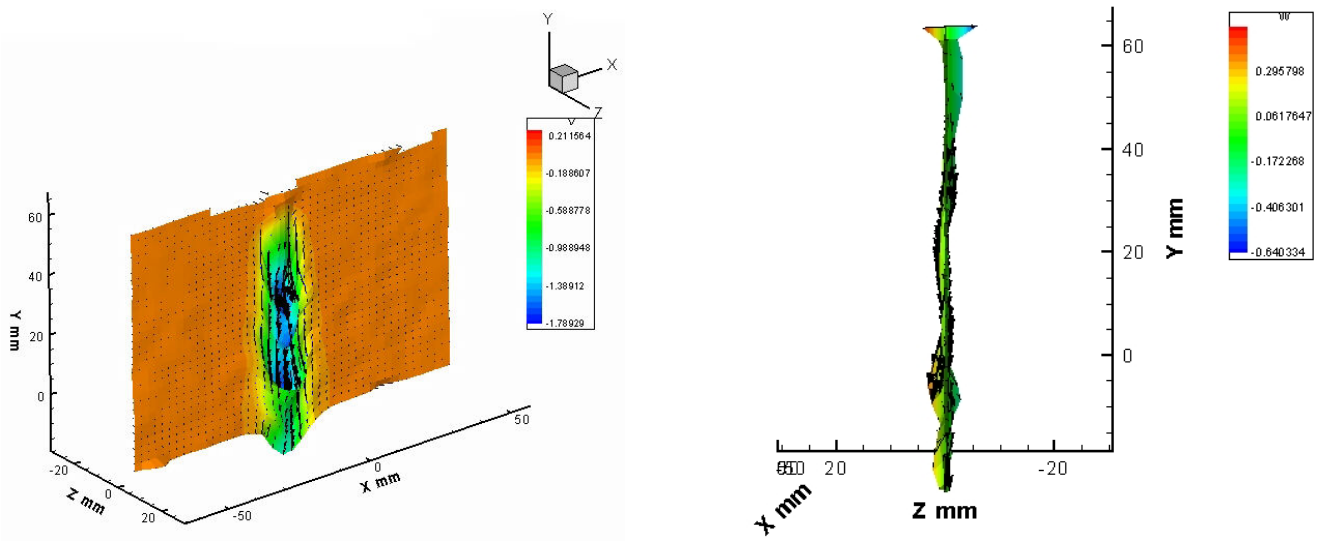

(a) 3 components velocity field (b) 3 C velocity field (y, z) (h = 230 mm V_{mean} = 1.8 m/s)

Fig. 14. Cross sectional three components velocity field.

It can be noticed that three dimensional (3D) velocity structures are observed in round since several years. Weisgraber (weisgraber, 1998) shown at the same Reynolds number in one streamwise plane (y_c/d_{inj} = 20) a "net entrainment of the surrounding fluid into the core". It's measurements reveal that this entrainment field structure disappears at higher Reynolds number (16,000) but it can be pointed out that there is an flow entrainment of surrounding fluid at Re = 16,000 very similar to our measurements (Fig. 7(b)). More recently Sakakibara (2005) found the same kind of three dimensional flows in similar conditions at lower Reynolds number.

Because the first region observed in the jet (called tube jet) is not conformed to those classically defined in a round jet injection, this particular structure could be associated to it. As a matter of fact, it is well known that the swirl flow is used to keep a constant shape of the flow as long as possible like in the tube jet region. But as it was previously observed (Wen, 2005), the insertion of a swirling strip generates a deflection angle larger than in the case of a jet with a tube without any insert. In our measurements from PIV/LIF the deflecting angle of the jet is nearly the same as it was defined from free jet. So, this 3D structure is probably not associated with a default from the line injection.

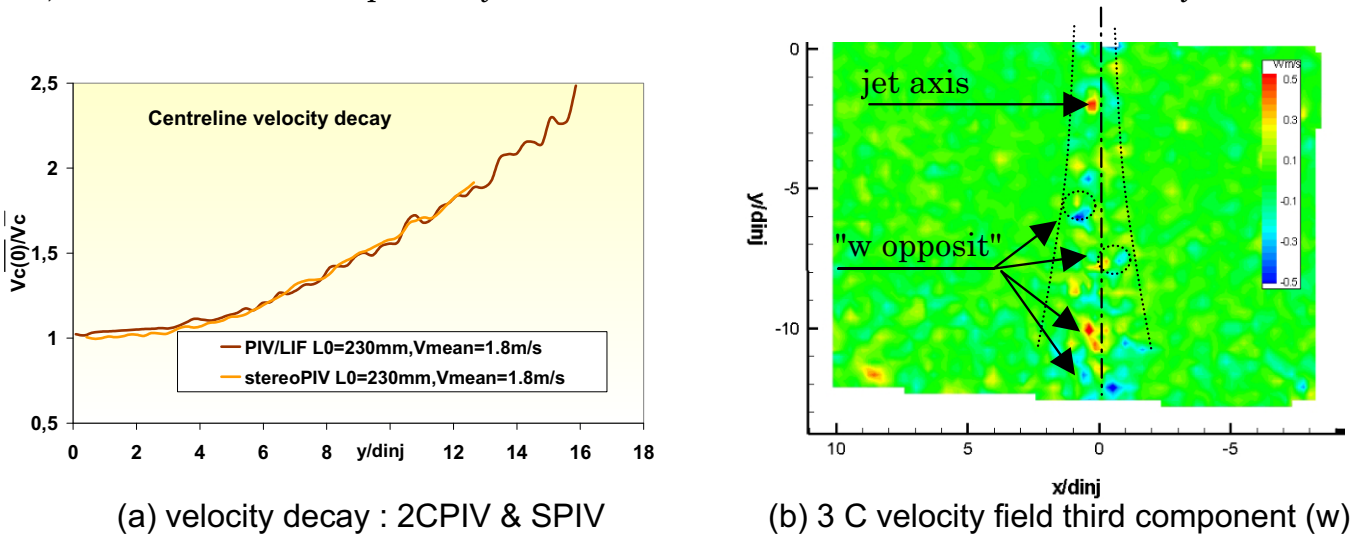

(a) velocity decay : 2CPIV & SPIV (b) 3 C velocity field third component (w)

Fig. 16. Three components velocity field (h = 230 mm V_{mean} = 1.8 m/s).

4. Conclusion

Experimental flow visualizations have been performed to investigate velocity and concentration fields during round jet injection into a square tank. Experiments have been carried out for two different velocity injections and two different nozzle-to-wall distances. Combined 2C PIV and LIF measurements have been conducted to analyze velocity and concentration fields in both the impinging and surrounding regions. A 3C PIV analysis has been also performed at the same conditions. The existence of the classical "deflecting" and "self similar" region have been verified by examining the mean velocity profiles. From the 10 % loci the concentration structure is build and a similar layer of radial diffusion is found.

A 3 dimensional velocity structure similar to a swirl injection has been observed from measurement for the present jet configuration. Since the deflecting angle of the jet is nearly the same as that defined for free jet, this structure is possibly not associated to swirl flow initiated from injection line. Further investigations are developed to analyze velocity and concentration fields in the plane normal to the jet axis.

References

Aanen, L., Telesca, A. and Westerweel, J., Measurement of turbulent mixing using PIV and LIF. Machine Graphics and vision, 8-4 (1999), 529-543.

Batchelor, G. K., An introduction to fluid dynamics, (2001), Cambridge University press.

Benayad, S., Salem, A. and Legrand, J., Study of mixing in an axisymmetric coflowing liquid jet by coupling L. D. A. to an electrochemical method, Journal of Applied electrochemistry, 30 (2000), 209-316.

Bian, S., Ceccio, S. L. and Driscoll, J. F., Simultaneous velocity/concentration measurements of a turbulent water jet using CPIV and CPLIF, 11th International Symposium on Flow Visualization (Notre Dame), (2004).

Bitting, J. W., Nikitopoulos, D. E., Gogineni S. P. and Gutmark, E. J., Visualization and 2 colors DPIV measurement of flows in circular and square coaxial nozzles, Experiments in Fluids, 31 (2001), 1-12.

Brossard, C., Bresson, A., Gicquel, P. and Grisch, F., Cartographies simultanées de vitesse, de température et de concentration par PIV et PLIF d'un jet d'air chaud ensemencé, 9ème Congrès Francophone de Vélocimétrie Laser A.3, 1 (2004), 14-17.

Deusch, S. and Dracos, T., Time resolved 3D passive scalar concentration-field imaging by laser induced fluorescence in moving liquids, Meas. Sci. Technol., 12 (2000), 188-200.

Chen, Y. C., Ma, C. F., Qin, M. and Li, Y. X., Theoretical study on impingement heat transfer with single-phase free-surface slot jets International Journal of Heat and Mass Transfer, 48 (2005) 3381-3386.

Dimotakis, P. E., Some issues on turbulent mixing and turbulence, Turbulence symposium in honor of W. C. Reynolds, Monterey, GALCIT report FM93-1, (1993).

Ding, R., Revstedt, J. and Fuchs, L., LIF study of mixing in circular impinging jets effects of boundary conditions, Proceedings of PSFVIP-4 (Chamonix), (2003), F4015.

Fondse, H., Leijdens, H. and Ooms, G., On the influence of the exit conditions on the entrainment rate in the development region of a free, round, turbulent jet, Applied Scientific Research, 40 (1983), 355-375.

Fujisawa, N., Nakamura, K. and Srinivas, K., Interaction of Two Parallel Plane Jets of Different Velocities, Journal of Visualization, 7-2 (2004), 135-142.

Fukushima, C., Aanen, L. and Westerweel, J., Simultaneous Velocity and Concentration Measurements of an Axisymmetric Turbulent Jet Using a Combined PIV/LIF, The Fifth JSME-KSME Fluids Engineering Conference (Nagoya, Japan) (2002).

Friehe, C. A., Van Atta C. W. and Gibson C. H., Jet turbulence: Dissipation rate measurements and correlations, In AGARD Turbulent shear flows (1971), CP-93, 18-1-18-7.

Guillard, F., Fritzon, R., Revstedt, J., Tägardh, C., Alden, M. and Fuchs L., Mixing in a confined turbulent impinging jet using planar laser-induced fluorescence, Experiments in Fluids, 25-2 (1998), 143-150.

Harran, G., Chassaing, P., Joly, L. and Chibat, M., Etude numérique des effets de densité dans un jet de mélange turbulent en microgravité, Rev Gén Therm, 35 (1996), 151-176.

Hu, H., Kobayashi, T., Saga, T., Segawa, S. and Taniguchi, N., Particle image velocimetry and planar laser-induced fluorescence measurements on lobed jet mixing flows, Experiments in Fluids suppl. (2000), S141-S157.

Hattori, H. and Nagano, Y., Direct Numerical Simulation of Turbulent Heat Transfer in Plane Impinging Jet, Int. Journal of Heat and Fluid Flow, 25-5 (2004), 749-758.

Koochesfahani, M., Cohn, R. and McKinnon, C., Simultaneous whole-field measurements of velocity and concentration fields using a combination of MTV and LIF,. Meas. Sci. Technol., 11 (2000), 1289-1300.

Law, A. W. K. and Wang, H., Measurement of mixing processes with combined digital particle image velocimetry and planar laser induced fluorescence, Exp. Thermal Fluid Sci., 22 (2000), 213-229.

Matin, H., Heat and mass transfer between impinging gas jets and solid surfaces, Adv. heat transfer, 13 (1977), 1-60.

Nishino, K., Samada, M., Kasuya, K. and Torii, K., Turbulence statistics in the stagnation region of an axisymmetric impinging jet flow, Int. Journal of Heat and Fluid Flow, 17-3 (1996), 193-201

Raffel, M., Willert, C. and Kompenhas, J., Particle Image Velocimetry: A practical guide, (1998), Springer -Verlag Berlin Heidelberg.

Sakakibara, J. and Hori, T., Three-dimensional vortical structures of a round impinging jet measured by scanning stereo-PIV, 6th Int. Symp. on Particle Image Velocimetry, (2005).

Saylor, J. R., Differential diffusion in turbulent and oscillatory nonturbulent, water flows, (1993), Ph. D. Thesis, Yale University.

Saylor, J. R. and Sreenivasan, K. R., Differential diffusion in low Reynolds number water jets,, Phys. Fluids, 10-5 (1998), 1135-1146.
Stricker, J. and Zakharin, B., 3-D Turbulent density field diagnostics by tomographic Moire, technique, Experiments in Fluids, 23 (1997), 76-85.
Su, L. K., Measurements of the three-dimensional scalar dissipation rate in gas-phase planar turbulent jets, Center for Turbulence Research Annual Research Briefs, (1998).
Tsurikov, M. S. and Clemens, N. T., Scalar/velocity imaging of the fine scales in gas-phase turbulent jets, American Institute of Aeronautics and Astronautics.
Webster, D. R., Roberts, P. J. W. and Ra'ad, L., Simultaneous DPTV/PLIF measurements of a turbulent jet, Experiments in Fluids, 30 (2001), 65-72.
Watanabe, Y., Hashizume, Y. and Fujisawa, N., Simultaneous Flow Visualization and PIV Measurement of Turbulent Buoyant Plume, Journal of Visualization, 8-4 (2005), 293-294.
Weisgraber, T. H. and Liepmann, D., Turbulent structure during transition to self-similarity in a round jet, Experiments in Fluids, 24 (1998), 210-224.

Author Profile

David Reungoat: He received his Ph D in Mechanical Engineering in 1994 from University of Poitiers. He has been working in Trefle Laboratory, Bordeaux University, since 1996 as a Lecturer. His research interests are Quantitative Visualization, PIV, PLIF, hydrodynamic interactions in complex fluid at low Reynolds number and Turbulent mixing.

Nicolas Rivière: He received his Dipl.-Ing. degree in Mechnical Engeneering from the graduate school of engineering ENSIETA (Brest, France) in 2004. He obtained his M. Sc. degree in Fluid Dynamics & Combustion from University of Poitiers in 2004. He is currently doing Ph. D. program in University of Bordeaux. His current research interests include quantitative visualization in fluid mechanics, PIV, LIF, hydrodynamic interactions and turbulent mixing.

Jean-Pierre Fauré: He received his Ph. D. in Mechanical Engineering from University of Bordeaux I in 1995. Since 1997 he has been working at CEA as engineer.